NeuroImage 67 (2013) 33–41

Contents lists available at SciVerse ScienceDirect

NeuroImage

journal homepage: www.elsevier.com/locate/ynimg

A robust variational approach for simultaneous smoothing and estimation of DTI

Meizhu Liu [a,*], Baba C. Vemuri [b], Rachid Deriche [c]

[a] Siemens Corporate Research & Technology, Princeton, NJ, 08540, USA
[b] Dept. of CISE, University of Florida, Gainesville, FL, 32611, USA
[c] Project-Team ATHENA, Inria Sophia Antipolis - Méditerranée, 06902, France

ARTICLE INFO

Article history:
Accepted 7 November 2012
Available online 17 November 2012

Keywords:
DTI estimation
Variational principle
Non-local means
Total Kullback–Leibler divergence
Diffusion MRI
Limited memory quasi-Newton method

ABSTRACT

Estimating diffusion tensors is an essential step in many applications — such as diffusion tensor image (DTI) registration, segmentation and fiber tractography. Most of the methods proposed in the literature for this task are not simultaneously statistically robust and feature preserving techniques. In this paper, we propose a novel and robust variational framework for simultaneous smoothing and estimation of diffusion tensors from diffusion MRI. Our variational principle makes use of a recently introduced total Kullback–Leibler (tKL) divergence for DTI regularization. tKL is a statistically robust dissimilarity measure for diffusion tensors, and regularization by using tKL ensures the symmetric positive definiteness of tensors automatically. Further, the regularization is weighted by a non-local factor adapted from the conventional non-local means filters. Finally, for the data fidelity, we use the nonlinear least-squares term derived from the Stejskal–Tanner model. We present experimental results depicting the positive performance of our method in comparison to competing methods on synthetic and real data examples.

Introduction

Diffusion weighted magnetic resonance imaging (MRI) is a very popular imaging technique that has been widely applied (Jones, 2010) in recent times. It uses diffusion sensitizing gradients to non-invasively capture the anisotropic properties of the tissue being imaged. Diffusion tensor imaging (DTI) approximates the diffusivity function by a symmetric positive definite tensor of order two (Basser et al., 1994). DTI is an MRI modality that provides information about the movement of water molecules in a tissue. DTI describes the diffusion direction of water molecules in the brain which is associated with the direction of fiber tracts in the white matter. When this movement is hindered by membranes and macromolecules, water diffusion becomes anisotropic. Therefore, in highly structured tissues such as nerve fibers, this anisotropy can be used to characterize the local structure of the tissue. Consequently, many applications are based on the estimated diffusion tensor fields, such as registration (Gur and Sochen, 2007; Jia et al., 2011; Wang et al., 2011; Yang et al., 2008; Yeo et al., 2009), segmentation (Descoteaux et al., 2008; Goh and Vidal, 2008; Hasan et al., 2007; Lenglet et al., 2006; Liu et al., 2007; Motwani et al., 2010; Savadjiev et al., 2008; Vemuri et al., 2011; Wang and Vemuri, 2005), atlas construction (Assemlal et al., 2011; Barmpoutis and Vemuri, 2009; Mori et al., 2008; Xie et al., 2010), anatomy modeling (Faugeras et al., 2004), fiber tract related applications (Burgela et al., 2006; Durrleman et al., 2011; Lenglet et al., 2009; Mori and van Zijl, 2002; Savadjiev et al., 2008; Wang et al., 2010, 2012; Zhu et al., 2011) and so on. All of these latter tasks will benefit from the estimation of smooth diffusion tensors.

Estimating the diffusion tensors (DTs) from DWI is a challenging problem, since the DWI data are invariably affected by noise during its acquisition process (Poupon et al., 2008b; Tang et al., 2009; Tristan-Vega and Aja-Fernandez, 2010). Therefore, a robust DTI estimation method which is able to perform a feature preserving denoising is desired. For most of the existing methods, the DTs are estimated by using the raw diffusion weighted echo intensity image (DWI). At each voxel of the 3D image lattice, the diffusion signal intensity S is related with its diffusion tensor $\mathbf{D}\in\mathbf{SPD}(3)$[1] via the Stejskal–Tanner equation (Stejskal and Tanner, 1965)

$$S = S_0 \exp\left(-b\mathbf{g}^T\mathbf{D}\mathbf{g}\right), \tag{1}$$

where S_0 is the signal intensity without diffusion, b is the b-value and $\mathbf{g}$ is the direction of the diffusion sensitizing gradient.

There are various methods (Barmpoutis et al., 2009a; Batchelor et al., 2005; Chang et al., 2005; Chefd'hotel et al., 2004; Fillard et al., 2007; Hamarneh and Hradsky, 2007; Mangin et al., 2002; Mishra et al., 2006; Niethammer et al., 2006; Pennec et al., 2006; Poupon et al., 2008b; Salvador et al., 2005; Tang et al., 2009; Tristan-Vega

* Corresponding author.
E-mail address: liufkmc@gmail.com (M. Liu).

[1] $\mathbf{SPD}(3)$ represents the space of 3×3 symmetric positive definite matrices.

1053-8119/$ – see front matter
http://dx.doi.org/10.1016/j.neuroimage.2012.11.012

and Aja-Fernandez, 2010; Tschumperle and Deriche, 2003, 2005; Vemuri et al., 2001; Wang et al., 2003, 2004) in existing literature, to estimate **D** from S. A very early one is a direct tensor estimation (Westin et al., 2002), which gives an explicit solution for **D** and S_0. Though time efficient, it is sensitive to noise because only 7 gradient directions are used to estimate **D** and S_0. Another method is the minimum recovery error (MRE) estimation or least squares fitting (Basser et al., 1994) which minimizes the error when recovering the DTs from the DWI. MRE is better than direct estimation because it uses more gradient directions, which increase its reliability. However, it does not smoothen the DWI or the DTI, and thus it is subject to noise in the input data.

With this in mind, many denoising frameworks (Gilboa et al., 2004; Spira et al., 2007) have been proposed to improve the signal to noise ratio (SNR). Some methods perform denoising on the DWI and then estimate the DTI. Typical approaches to DWI denoising are designed according to the statistical properties of the noise. Most of these approaches assume that the noise follows the Rician distribution (Descoteaux et al., 2008; Koay and Basser, 2006; Landman et al., 2007; Piurica et al., 2003), and when denoising, they use the second order moment of the Rician noise (McGibney and Smith, 1993), maximum likelihood (ML) (Sijbers and den Dekker, 2004) and expectation maximization (EM) approaches (DeVore et al., 2000; Marzetta, 1995), wavelets (Nowak, 1999), anisotropic Wiener filtering (Martin-Fernandez et al., 2007), total variation schemes (McGraw et al., 2004), Markov random fields (Zhang et al., 2001), nonparametric neighborhood statistics techniques like non-local means (NLM) (Awate and Whitaker, 2005; Coupe et al., 2008) and unbiased NLM (Manjon et al., 2008; Wiest-Daessle et al., 2008) algorithms, Perona–Malik-like smoothing (Basu et al., 2006) or the linear minimum mean square error (LMMSE) scheme (Aja-Fernandez et al., 2008).

Alternatively, some methods first estimate the diffusion tensors from the raw DWI and then perform denoising on the tensor field (Moraga et al., 2007). One representative method is by using the NLM framework incorporating a log-Euclidean metric (Fillard et al., 2005). The drawback of such two-stage processes is that the errors might be accumulated from one stage to the other.

Bearing these deficiencies in mind, researchers developed a variational framework (VF) based estimation (Chefd'hotel et al., 2004; Tschumperle and Deriche, 2003; Wang et al., 2003, 2004). These approaches take into account the SPD (symmetric positive definite) constraint on the diffusion tensors. The smoothing in all these approaches involves some kind of weighted averaging over neighborhoods which define the smoothing operators resulting from the variational principles. Some of these smoothing operators are locally defined and do not capture global geometric structure present in the image. Moreover, they are not statistically robust.

To overcome the aforementioned drawbacks, we propose a novel statistically robust variational non-local approach for simultaneous smoothing and tensor estimation from the raw DWI data. This approach combines the variational framework, non-local means and a statistically robust regularizer on the tensor field. The main contributions of this approach are three-fold. First, we use a statistically robust divergence measure total Bregman divergence to regularize the smoothness measure on the tensor field. Combined with the Cholesky decomposition of the diffusion tensors, this automatically ensures the positive definiteness of the estimated diffusion tensors, which overcomes the common problem for many techniques that manually force the tensor to be positive definite or resort to accuracy of finite precision arithmetic leading to the equivalence between testings for positive definiteness and positive semidefiniteness as in Wang et al. (2003, 2004). Second, it uses an adaptation of the NLM to find the weight for the smoothness regularization terms. This preserves the global structure of the tensor field while denoising. Finally, it achieves simultaneous denoising and DTI estimation, which is able to avoid the error propagation of a two stage approach described earlier. Besides, this method can be easily extended to a higher order tensor estimation. We will explain these points at length in the rest of the paper.

The rest of the paper is organized as follows. In the Proposed method section, we introduce our proposed method, followed by the empirical validation in the Experiments section. Finally we conclude.

Proposed method

Our proposed integrated variational non-local approach has three components, minimizing the data fidelity error, smoothing over S_0 and the tensor field. The proposed model is given by the following equation:

$$\begin{aligned}&\min_{S_0,\mathbf{D}\in\mathbf{SPD}} \mathbf{E}(S_0,\mathbf{D})\\ &=(1-\alpha-\beta)\int_\Omega \sum_{i=1}^{n}\left(S_i-S_0\exp\left(-b\mathbf{g}_i^T\mathbf{D}\mathbf{g}_i\right)\right)^2 d\mathbf{x}\\ &+\alpha\int_\Omega\int_{\mathcal{V}(\mathbf{x})} w_1(\mathbf{x},\mathbf{y})(S_0-S_0(\mathbf{y}))^2 d\mathbf{y}d\mathbf{x}\\ &+\beta\int_\Omega\int_{\mathcal{V}(\mathbf{x})} w_2(\mathbf{x},\mathbf{y})\delta(\mathbf{D},\mathbf{D}(\mathbf{y}))d\mathbf{y}d\mathbf{x},\end{aligned}\tag{2}$$

where Ω is the domain of the image, n is the number of diffusion gradients, $\mathcal{V}(\mathbf{x})$ is the search window at voxel $\mathbf{x}$, and $\delta(\mathbf{D}, \mathbf{D}(\mathbf{y}))$ is the total Kullback–Leibler (tKL) divergence (Vemuri et al., 2011) between tensors **D** and $\mathbf{D}(\mathbf{y})$ which will be explained in detail later. The first term captures the non-linear data fitting error, the second and third terms are smoothness constraints on S_0 and **D**. α and β are constants balancing the fitting error and the smoothness.[2] $w_1(\mathbf{x},\mathbf{y})$ and $w_2(\mathbf{x},\mathbf{y})$ are the regularization weights for S_0 and **D**. Since S_0 and S are linearly related, while **D** and S are "logarithmically" related, so we use different methods to calculate $w_1(\mathbf{x},\mathbf{y})$ and $w_2(\mathbf{x},\mathbf{y})$. Note, S_i, S_0 and **D** by default represent the values at voxel $\mathbf{x}$, unless specified otherwise.

The discrete case of Eq. (2) is

$$\begin{aligned}&\min_{S_0,\mathbf{D}\in\mathbf{SPD}} \mathbf{E}(S_0,\mathbf{D})\\ &=(1-\alpha-\beta)\sum_{\mathbf{x}\in\Omega} \sum_{i=1}^{n}\left(S_i-S_0\exp\left(-b\mathbf{g}_i^T\mathbf{D}\mathbf{g}_i\right)\right)^2\\ &+\alpha\sum_{\mathbf{x}\in\Omega}\sum_{\mathbf{y}\in\mathcal{V}(\mathbf{x})} w_1(\mathbf{x},\mathbf{y})(S_0-S_0(\mathbf{y}))^2\\ &+\beta\sum_{\mathbf{x}\in\Omega}\sum_{\mathbf{y}\in\mathcal{V}(\mathbf{x})} w_2(\mathbf{x},\mathbf{y})\delta(\mathbf{D},\mathbf{D}(\mathbf{y})).\end{aligned}\tag{3}$$

Since most of the time, DTI estimation problems are in the discrete case, we will focus on the discrete case in this work.

Computation of the weights $w_1(\mathbf{x},\mathbf{y})$ and $w_2(\mathbf{x},\mathbf{y})$

$w_1(\mathbf{x},\mathbf{y})$ and $w_2(\mathbf{x},\mathbf{y})$ are the regularization weights of the smoothness terms. If $w_1(\mathbf{x},\mathbf{y})$ is large, it requires S_0 and $S_0(\mathbf{y})$ to be similar. Similarly, if $w_2(\mathbf{x},\mathbf{y})$ is large, it requires **D** and $\mathbf{D}(\mathbf{y})$ to be similar. Usually, one requires S_0's and **D**'s to be respectively similar only if the corresponding diffusion signals are similar. We will compute $w_1(\mathbf{x},\mathbf{y})$ and $w_2(\mathbf{x},\mathbf{y})$ according to the statistical properties of the diffusion weighted signals. It has been recognized that the diffusion signal S follows the Rician distribution (Descoteaux et al., 2008; Koay and Basser, 2006; Piurica et al., 2003), i.e.,

$$p\left(S;\bar{S},\sigma^2\right)=\frac{S}{\sigma^2}\exp\left(-\frac{S^2+\bar{S}^2}{2\sigma^2}\right)I_0\left(\frac{S\bar{S}}{\sigma^2}\right),\tag{4}$$

[2] Usually, the noisier the image, the larger will α and β be, and vice-versa. The noise in the images can be estimated by using any of the popular methods described in Aja-Fernandez et al. (2009) and Tristan-Vega and Aja-Fernandez (2010).

where $\bar{S}$ is the signal without noise, σ is the variance of the Rician noise. Since S_0 is linearly related with S and $\mathbf{D}$ is "logarithmically" related with S, we set the regularization weights for S_0 and $\mathbf{D}$ to be

$$w_1(\mathbf{x},\mathbf{y}) = \frac{1}{Z_1(\mathbf{x})}\exp\left(\frac{-\|S(\mathcal{N}(\mathbf{x}))-S(\mathcal{N}(\mathbf{y}))\|^2}{h\sigma^2}\right), \tag{5}$$

$$w_2(\mathbf{x},\mathbf{y}) = \frac{1}{Z_2(\mathbf{x})}\exp\left(\frac{-\|\log S(\mathcal{N}(\mathbf{x}))-\log S(\mathcal{N}(\mathbf{y}))\|^2}{h\sigma^2}\right), \tag{6}$$

where Z_1 and Z_2 are normalizers, h is the filtering parameter (Coupe et al., 2006), and σ is the standard variation of the noise, which is estimated by using the first mode of the background (Aja-Fernandez et al., 2009; Tristan-Vega and Aja-Fernandez, 2010). $\mathcal{N}(\mathbf{x})$ and $\mathcal{N}(\mathbf{y})$ denote the neighborhoods of $\mathbf{x}$ and $\mathbf{y}$ respectively. The neighborhood of $\mathbf{x}$ can be viewed as the voxels around $\mathbf{x}$ or a square centered at $\mathbf{x}$ with a user defined radius. Furthermore,

$$\|S(\mathcal{N}(\mathbf{x}))-S(\mathcal{N}(\mathbf{y}))\|^2 = \sum_j^m \left\| S\left(\mu_j\right)-S\left(\nu_j\right)^2\right\|, \text{ and}$$
$$\|\log S(\mathcal{N}(\mathbf{x}))-\log S(\mathcal{N}(\mathbf{y}))\|^2 = \sum_j^m \left\|\log S\left(\mu_j\right)-\log S\left(\nu_j\right)\right\|^2,$$

where μ_j and ν_j are the jth voxels in the neighborhoods $\mathcal{N}(\mathbf{x})$ and $\mathcal{N}(\mathbf{y})$ respectively, and m is the number of voxels in each neighborhood.

From Eq. (5), we can see that if the signal intensities for two voxels are similar, $w_1(\mathbf{x,y})$ and $w_2(\mathbf{x,y})$ are large. Consequently according to Eq. (3), S_0 and $S_0(\mathbf{y})$, $\mathbf{D}$ and $\mathbf{D}(\mathbf{y})$ should be similar respectively.

NLM is known for its high accuracy and high computational complexity. To address the computational load problem, we use two methods. One is to decrease the number of computations performed by selecting voxels in the search window, and the other is to make use of parallel computing. Concretely, we will prefilter the voxels in the search window which are not similar to the voxel under consideration if their diffusion weighted signal intensities are not similar. This is specified as

$$w_1(\mathbf{x},\mathbf{y}) = \begin{cases} \frac{1}{Z_1(\mathbf{x})}\exp\left(\frac{-\|S(\mathcal{N}(\mathbf{x}))-S(\mathcal{N}(\mathbf{y}))\|^2}{h\sigma^2}\right), \\ \text{if } \frac{\|S(\mathcal{N}(\mathbf{x}))\|^2}{\|S(\mathcal{N}(\mathbf{y}))\|^2}\in[\tau_1,\tau_2] \\ 0, \quad \text{Otherwise} \end{cases}.$$

$$w_2(\mathbf{x},\mathbf{y}) = \begin{cases} \frac{1}{Z_2(\mathbf{x})}\exp\left(\frac{-\|\log S(\mathcal{N}(\mathbf{x}))-\log S(\mathcal{N}(\mathbf{y}))\|^2}{h\sigma^2}\right), \\ \text{if } \frac{\|S(\mathcal{N}(\mathbf{x}))\|^2}{\|S(\mathcal{N}(\mathbf{y}))\|^2}\in[\tau_1,\tau_2] \\ 0, \quad \text{Otherwise} \end{cases}.$$

τ_1 and τ_2 are the thresholds for prefiltering. We set $\tau_1 = 0.1$ and $\tau_2 = 10$ in our experiments.

In the context of parallel computing, we divide the computations into smaller parts and assign the computations to several processors. Since the smaller parts for NLM are not correlated, thus it can improve the efficiency a lot by using parallel computing. In our case, we divide the volumes into 8 subvolumes, and assign each subvolume to one processor, and a desktop with 8 processors is used. This multi-threading technique greatly enhances the efficiency.

Computation of the tKL divergence

tKL divergence is a special case of the recently proposed total Breman divergence (tBD) (Liu et al., 2010; Vemuri et al., 2011). This divergence measure is based on the orthogonal distance between the convex generating function of the divergence and its tangent approximation at the second argument of the divergence. The *total Bregman divergence* δ_f associated with a real valued strictly convex and differentiable function f defined on a convex set X between points $x, y \in X$ is defined as,

$$\delta_f(x,y) = \frac{f(x)-f(y)-\langle x-y, \nabla f(y)\rangle}{\sqrt{1+\|\nabla f(y)\|^2}}, \tag{7}$$

where $\langle\cdot,\cdot\rangle$ is the inner product, and $\|\nabla f(y)\|^2 = \langle\nabla f(y), \nabla f(y)\rangle$ generally. tBD has been proven to have the property of being intrinsically robust to noise and outliers. Furthermore, it yields a closed form formula for computing the median (an ℓ_1-norm average) for a set of symmetric positive definite tensors. When $f(x) = -\log x$ and X is the set of probability density functions (pdf), Eq. (7) becomes the tKL divergence, which is

$$\delta_f(x,y) = \frac{\int x \log\frac{x}{y}}{\sqrt{1+\int y(1+\log y)^2}}. \tag{8}$$

Motivated by an earlier use of the tKL divergence as a dissimilarity measure between DTs for DTI segmentation (Vemuri et al., 2011), we use tKL to measure the dissimilarity between tensors and apply it in the DTI regularization. It has been shown that the tKL divergence (Vemuri et al., 2011) based ℓ_1-norm average, termed by the t-center, is invariant to special linear group transformations (denoted by $SL(n)$).[3] This is detailed in the following.

Since order-2 SPD tensors can be seen as covariance matrices of zero mean Gaussian pdf (Wang et al., 2004). Let $\mathbf{P}, \mathbf{Q} \in \mathbf{SPD}(l)$, then their corresponding pdf are

$$p(\mathbf{t};\mathbf{P}) = \frac{1}{\sqrt{(2\pi)^l det\mathbf{P}}}\exp\left(-\frac{\mathbf{t}^T\mathbf{P}^{-1}\mathbf{t}}{2}\right),$$
$$q(\mathbf{t};\mathbf{Q}) = \frac{1}{\sqrt{(2\pi)^l det\mathbf{Q}}}\exp\left(-\frac{\mathbf{t}^T\mathbf{Q}^{-1}\mathbf{t}}{2}\right),$$

and the tKL between them is explicitly given by,

$$\delta(\mathbf{P},\mathbf{Q}) = \frac{\int p\log\frac{p}{q}d\mathbf{t}}{\sqrt{1+\int(1+\log q)^2 q d\mathbf{t}}} = \frac{\log\left(\det\left(\mathbf{P}^{-1}\mathbf{Q}\right)\right)+tr\left(\mathbf{Q}^{-1}\mathbf{P}\right)-l}{2\sqrt{c_1+\frac{(\log(\det\mathbf{Q}))^2}{4}-c_2\log(\det\mathbf{Q})}},$$

where $c_1 = \frac{3l}{4}+\frac{l^2\log 2\pi}{2}+\frac{(l\log 2\pi)^2}{4}$ and $c_2 = \frac{l(1+\log 2\pi)}{2}$.

Moreover, the partial minimization of the third term in Eq. (3)

$$\min_{\mathbf{D}} \sum_{\mathbf{y}\in\mathbb{V}(\mathbf{x})} \delta(\mathbf{D},\mathbf{D}(\mathbf{y}))$$

leads to the t-center for the set of $\mathbf{D}(\mathbf{y})$. The t-center has been well studied in Vemuri et al. (2011). Given a set of tensors $\{\mathbf{Q}_i\}$, the t-center $\mathbf{P}^*$ minimizes the ℓ_1-norm divergence to all the tensors, i.e.,

$$\mathbf{P}^* = \arg\min_{\mathbf{P}} \sum_i \delta(\mathbf{P},\mathbf{Q}_i), \tag{9}$$

[3] An $n\times n$ matrix $A\in SL(n)$ implies $\det(A)=1$.

and $\mathbf{P}^*$ is explicitly expressed as

$$\mathbf{P}^* = \left(\sum_i \frac{a_i}{\sum_j a_j}\mathbf{Q}_i^{-1}\right)^{-1}, \quad a_i = \left(2\sqrt{c_1 + \frac{(\log(\det\mathbf{Q}_i))^2}{4} - c_2\log(\det\mathbf{Q}_i)}\right)^{-1}. \tag{10}$$

The t-center for a set of DTs is the weighted harmonic mean, which is in closed form. Moreover, the weight is invariant to $SL(n)$ transformations, i.e., $a_i(\mathbf{Q}_i) = a_i(\mathbf{A}^T\mathbf{Q}_i\mathbf{A})$, $\forall \mathbf{A} \in SL(n)$. The t-center after the transformation becomes

$$\hat{\mathbf{P}}^* = \left(\sum a_i\left(\mathbf{A}^T\mathbf{Q}_i\mathbf{A}\right)^{-1}\right)^{-1} = \mathbf{A}^T\mathbf{P}^*\mathbf{A}. \tag{11}$$

This means that if $\{\mathbf{Q}_i\}_{i=1}^m$ are transformed by some member of $SL(n)$, the t-center will undergo the same transformation. It was also found that the t-center will be robust to noise in that the weight will be smaller if the tensor has more noise (Vemuri et al., 2011). These properties make it an appropriate tool for the DTI applications.

The SPD constraint

It is known that if a matrix $\mathbf{D} \in \mathbf{SPD}$, there exists a unique lower diagonal matrix $\mathbf{L}$ with its diagonal values all positive, and $\mathbf{D} = \mathbf{LL}^T$ (Golub and Loan, 1996). This is the well known Cholesky factorization theorem. Wang et al. (2003, 2004) were the first to use Cholesky factorization to enforce the positive definiteness condition on the estimated smooth diffusion tensors from the DWI data. They use the argument that testing for positive definiteness is equivalent to testing for positive semidefiniteness under finite precision arithmetic and hence their cost function minimization is set on the space of positive semidefinite matrices, which is a closed set that facilitates the existence of a solution within that space. Unlike (Wang et al. (2003, 2004), we use Cholesky decomposition and tKL divergence to regularize the smoothness of the tensor field, and this automatically ensures the diagonal values of $\mathbf{L}$ to be positive. This argument is validated as follows.

Substituting $\mathbf{D} = \mathbf{LL}^T$ into Eq. (9), we get

$$\delta(\mathbf{L}, \mathbf{L}(\mathbf{y})) = \frac{\sum_{i=1}^3(\log\mathbf{L}_{ii}(\mathbf{y}) - \log\mathbf{L}_{ii}) + tr\left(\mathbf{L}^{-T}(\mathbf{y})\mathbf{L}^{-1}(\mathbf{y})\mathbf{LL}^T\right) - 1.5}{\sqrt{c_1 + \frac{\left(\sum_{i=1}^3\log\mathbf{L}_{ii}(\mathbf{y})\right)^2}{4} - c_2\sum_{i=1}^3\log\mathbf{L}_{ii}(\mathbf{y})}}. \tag{12}$$

Because by using the "*log*" function in the computation, Eq. (12) automatically requires $\mathbf{L}_{ii}s$ to be positive, therefore we do not need to manually force the tensor to be SPD. The detailed explanation is given in Appendix A.

Numerical solution

In this section, we present the numerical solution to the variational principle (3). The partial derivative equations of Eq. (3) with respect to S_0 and $\mathbf{L}$ can be computed explicitly and are,

$$\begin{aligned}\frac{\partial\mathbf{E}}{\partial S_0} &= -2(1-\alpha-\beta)\sum_{i=1}^n v_i - 2\alpha\sum_{\mathbf{y}\in\mathbb{V}(\mathbf{x})} w_1(\mathbf{x},\mathbf{y})(S_0 - S_0(\mathbf{y})),\\ \frac{\partial\mathbf{E}}{\partial\mathbf{L}} &= 4(1-\alpha-\beta)\sum_{i=1}^n bS_0 v_i\mathbf{L}^T\mathbf{g}_i\mathbf{g}_i^T\\ &\quad -2\beta\sum_{\mathbf{y}\in\mathbb{V}(\mathbf{x})}\frac{w_2(\mathbf{x},\mathbf{y})\left(\mathbf{L}^{-1} - \mathbf{L}^T\mathbf{L}^{-T}(y)\mathbf{L}^{-1}(y)\right)}{\sqrt{c_1 + \frac{\left(\sum_{i=1}^3\log\mathbf{L}_{ii}(\mathbf{y})\right)^2}{4} - c_2\sum_{i=1}^3\log\mathbf{L}_{ii}(\mathbf{y})}},\end{aligned} \tag{13}$$

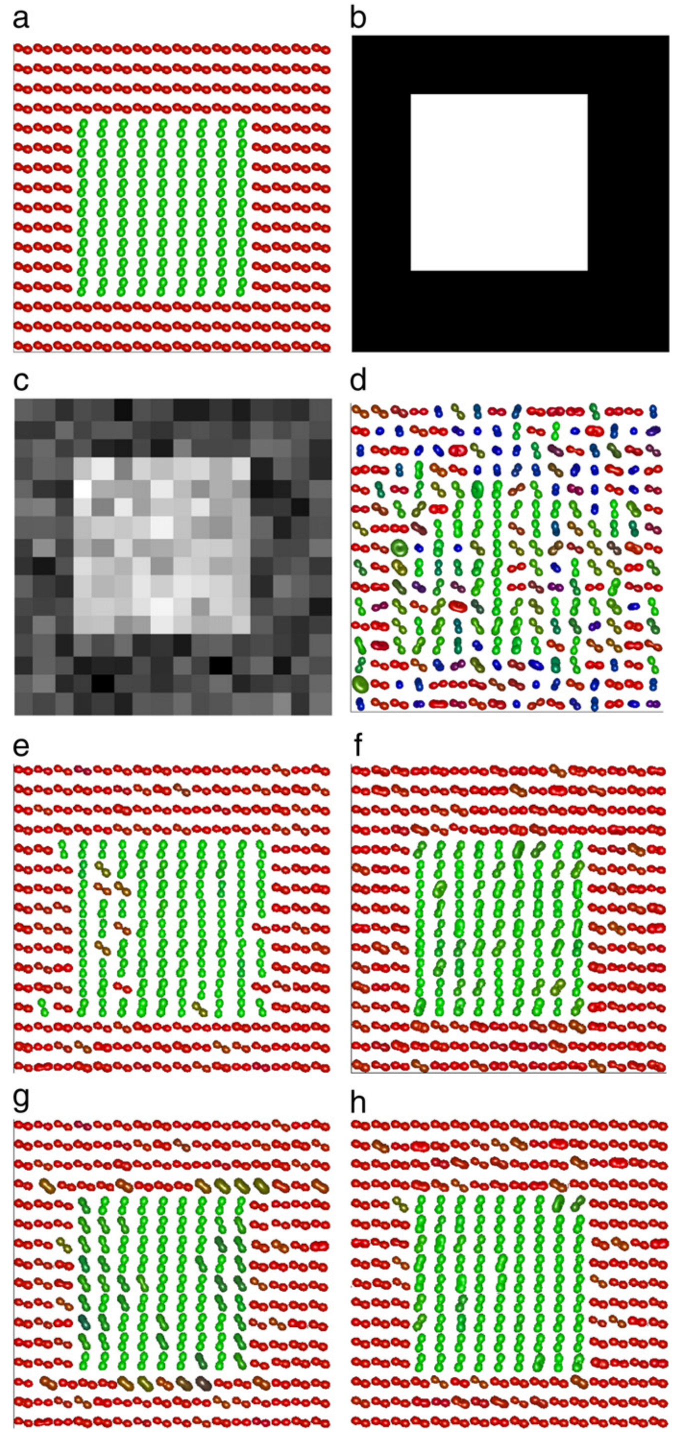

Fig. 1. (a) Ground truth synthetic DTI field, (b) the original DWI corresponding to $\mathbf{g}_1$, (c) the Rician noise affected DWI, the DTI estimation by using (d) MRE, (e) VF, (f) LMMSE, (g) NLM, and (h) the proposed technique.

where

$$v_i = \left(S_i - S_0\exp\left(-b\mathbf{g}_i^T\mathbf{LL}^T\mathbf{g}_i\right)\right)\exp\left(-b\mathbf{g}_i^T\mathbf{LL}^T\mathbf{g}_i\right). \tag{14}$$

To solve Eq. (13), we use the limited memory quasi-Newton method described in Nocedal and Wright (2000). This method is useful for solving large problems with a lot of variables, as is in our case. This method maintains simple and compact approximations of Hessian matrices making them require, as the name suggests, modest

Table 1
Error in estimated DTI and S_0, by using different methods, from synthetic DWI with different levels of noise.

SNR	Error	MRE	VF	LMMSE	NLM	Proposed	$\alpha=0$	$\beta=0$
50	ϵ_θ	0.204 ± 0.064	0.107 ± 0.038	0.096 ± 0.060	0.085 ± 0.054	0.082 ± 0.045	0.112 ± 0.049	0.179 ± 0.062
	ϵ_{S_0}	0.269 ± 0.138	0.217 ± 0.106	0.208 ± 0.080	0.191 ± 0.112	0.133 ± 0.103	0.171 ± 0.098	0.224 ± 0.082
40	ϵ_θ	0.550 ± 0.351	0.275 ± 0.312	0.203 ± 0.304	0.195 ± 0.301	0.108 ± 0.102	0.169 ± 0.192	0.539 ± 0.348
	ϵ_{S_0}	0.584 ± 0.354	0.278 ± 0.359	0.215 ± 0.320	0.216 ± 0.328	0.140 ± 0.226	0.218 ± 0.225	0.542 ± 0.355
30	ϵ_θ	0.588 ± 0.359	0.434 ± 0.394	0.230 ± 0.363	0.217 ± 0.348	0.144 ± 0.130	0.214 ± 0.251	0.570 ± 0.359
	ϵ_{S_0}	0.753 ± 0.441	0.485 ± 0.370	0.282 ± 0.401	0.275 ± 0.352	0.173 ± 0.231	0.286 ± 0.432	0.607 ± 0.451
15	ϵ_θ	0.727 ± 0.561	0.504 ± 0.388	0.396 ± 0.426	0.384 ± 0.422	0.218 ± 0.252	0.372 ± 0.283	0.711 ± 0.577
	ϵ_{S_0}	0.968 ± 0.570	0.622 ± 0.517	0.479 ± 0.482	0.478 ± 0.457	0.235 ± 0.272	0.481 ± 0.474	0.921 ± 0.580
7	ϵ_θ	1.092 ± 0.595	0.688 ± 0.656	0.460 ± 0.526	0.519 ± 0.469	0.265 ± 0.276	0.457 ± 0.472	1.001 ± 0.591
	ϵ_{S_0}	1.334 ± 1.094	0.827 ± 0.680	0.543 ± 0.583	0.562 ± 0.554	0.273 ± 0.283	0.592 ± 0.57	1.306 ± 1.095

storage, besides yielding a linear rate of convergence. Specifically, we use the linear Broyden–Fletcher–Goldfarb–Shanno (L-BFGS) method (Nocedal and Wright, 2000) to construct the Hessian approximation.

Experiments

We evaluated our method on synthetic datasets with various levels of noise, and real datasets, including rat spinal cord datasets and human brain datasets. Based on the estimated tensor fields by using the technique presented in this paper, we achieved DTI segmentation for the rat spinal cord datasets, and some preliminary fiber tracking on human brain datasets. However, since the main thrust of this paper is the estimation of smooth diffusion tensor fields, the segmentation and fiber tracking results are not presented here.

We compared our method with other state-of-the-art techniques including VF (Tschumperle and Deriche, 2003), NLM (Wiest-Daessle et al., 2008) and LMMSE (Tristan-Vega and Aja-Fernandez, 2010) respectively. We also presented the MRE method for comparison since several software packages (3DSlicer 3.6[4] and fanDTasia (Barmpoutis et al., 2009b)) use this technique due to its simplicity. We implemented VF by ourselves since we did not find any open source versions on the web. For LMMSE, we used the implementation in a 3DSlicer 3.6. For NLM, we used an existing code[5] for DWI denoising and used our own implementation of the least squares fitting to estimate DTI from the denoised DWI. To ensure fairness, we tuned all the parameters of each method for every experiment, and chose the set of parameters yielding the best results. The visual and numerical results show that our method yields better results than the competing methods.

DTI estimation from synthetic datasets

There are two groups of synthetic datasets. The first one is a 16×16 DTI with two homogeneous regions as shown in Fig. 1(a). Each region is a repetition of a tensor, and the two tensors are $\mathbf{D}_1=[3.3,1.8,1.3,0,0,1.2]'$ and $\mathbf{D}_2=[3, 2.2, 3, -1, 0, 0]'$.[6] To generate the DWI based on this DTI, we let $S_0=5$, $b=1500s/\text{mm}^2$, and $\mathbf{g}$ be 22 uniformly-spaced directions on the unit sphere starting from (1,0,0). Substituting the DTI, S_0, b, $\mathbf{g}$ into the Stejskal–Tanner equation, we generate a $16\times16\times22$ DWI $\mathbf{S}$. One representative slice of $\mathbf{S}$ is shown in Fig. 1(b). Then following the method proposed in Koay and Basser (2006), we add the Rician noise to $\mathbf{S}$ and get $\tilde{\mathbf{S}}$, by using the formula $\tilde{S}(\mathbf{x})=\sqrt{(S(\mathbf{x})+n_r)^2+n_i^2}$, where n_r, $n_i\sim N(0,\sigma^2)$. By varying σ, we get different levels of noise and therefore a wide range of SNR ($\text{SNR}=\frac{mean(\mathbf{S})}{\sigma}$).

In our experiments, we set $\alpha=0.1$ and $\beta=0.4$. The search window size is set to be 25 and the neighborhood size is 9. Fig. 1(c) shows the slice in Fig. 1(b) after adding noise (SNR=60). The estimated DTI from using MRE, VF, NLM, LMMSE and the proposed method are shown in Fig. 1. The figure visually depicts that our method can estimate the tensor field more accurately.

To quantitatively assess the proposed variational unified model, we determine the accuracy of the computed principle eigenvectors of the tensors. Let ϵ_θ be the average angle between the principle eigenvectors of the estimated tensor field and the original known tensor field. Besides we compare the difference, denoted as ϵ_{S_0}, between the estimated and ground truth S_0. The results are shown in Table 1, from which it is evident that our method outperforms others and the significance in performance is more evident at higher noise levels. Even though the accuracy of NLM and our proposed method is very similar at high SNR, however, our method is much more computationally efficient than NLM. The average CPU time taken to converge for our method on a desktop computer with Intel 8 Core 2.8 GHz, 24 GB of memory, GNU Linux and MATLAB (Version 2010a) is 3.51 s, whereas, NLM requires 5.26 s (note both methods are executed by using multi-core processors).

We also evaluated the importance of the two regularization terms separately. $\alpha=0$ means removing the regularization on S_0, while $\beta=0$ means removing the regularization on $\mathbf{D}$. For these two cases, we evaluate the ϵ_θ and ϵ_{S_0}, and the results are shown in the last two columns of Table 1. The results show that removing either the regularization term will increase the DTI estimation error. This implies that both regularization terms are necessary in order to get accurate estimation results.

We also evaluated our method on the 64×64 fibercup dataset (Fillard et al., 2011; Poupon et al., 2008a) with a voxel size of $3\times3\times3$ mm^3, a b-value of $1500s/\text{mm}^2$ and 130 gradient directions. For the parameter settings in the proposed model, we chose $\alpha=0.1$ and $\beta=0.4$. The search window size is 9 and the neighborhood size is 4. We showed the estimated S_0, D11, D12, D13, D22, D23, D33, FA and the visualization of the estimated DTI by using fanDTasia (Barmpoutis et al., 2009a) in Fig. 2. The results depict that the proposed method can give a well smoothened and feature preserved tensor field.

DTI estimation from real datasets

We also did DTI estimation on a $100\times80\times32\times52$ 3D rat brain DWI. The data was acquired by using a PGSE technique with TR=1.5 s, TE=28.3 ms, bandwidth=35Khz, 52 diffusion weighted images with a b-value of 1334 s/mm^2.

We compared with several other methods on the DTI estimation, however, to save space, we only show the results of MRE, LMMSE and our proposed method. We present D11, D22, D33, S_0, FA, and mean trace for each estimated result. The DTI estimation results of MRE, LMMSE and our proposed method are shown in Figs. 3, 4 and 5 respectively.

We used a human brain DWI dataset ($256\times256\times72$) provided by Alfred Anwander of the Max Planck Institute for Human Neuroscience (Makuuchi et al., 2009). The DWIs were acquired with a whole-body 3 T Magnetom TRIO operating at 3 T (Siemens Medical Solutions)

[4] http://www.slicer.org/.
[5] https://www.irisa.fr/visages/benchmarks/.
[6] $\mathbf{D}$ is written as [D11,D22,D33,D12,D23,D13].

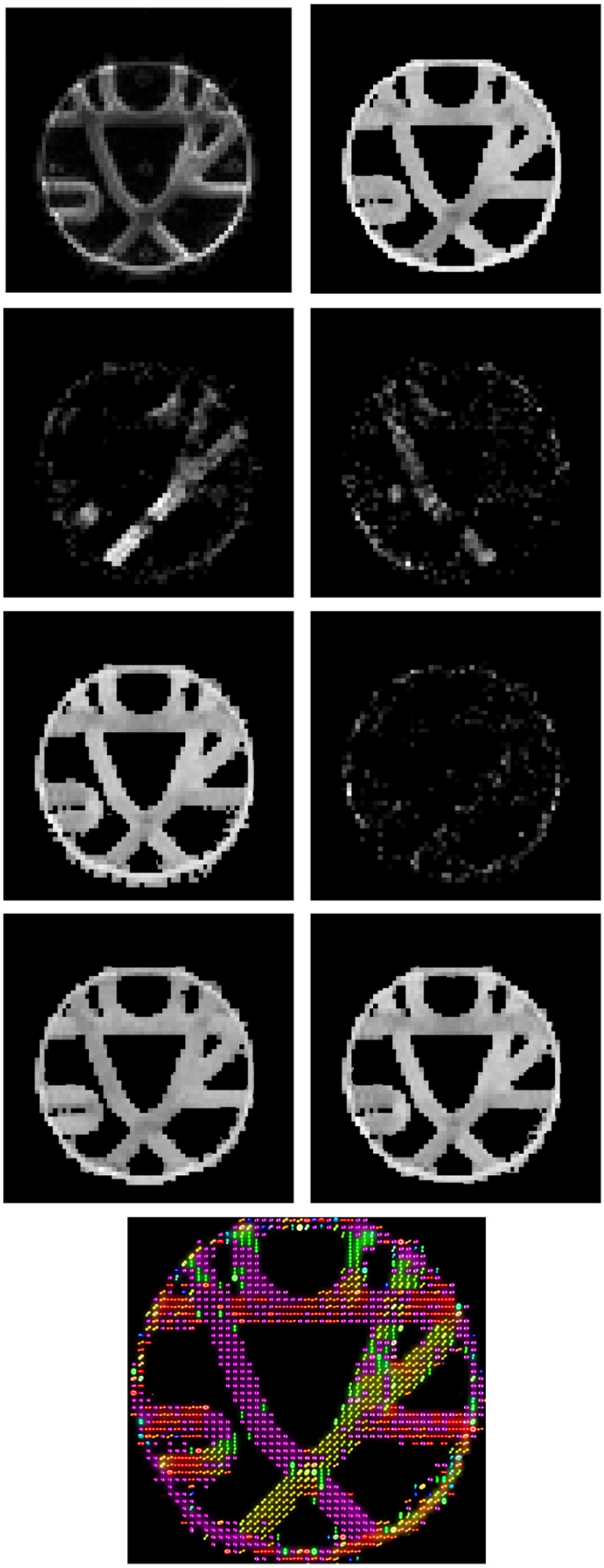

Fig. 2. From left to right, top to bottom are the estimated S_0, D11, D12, D13, D22, D23, D33, FA and the visualization of the estimated DTI by using fanDTasia.

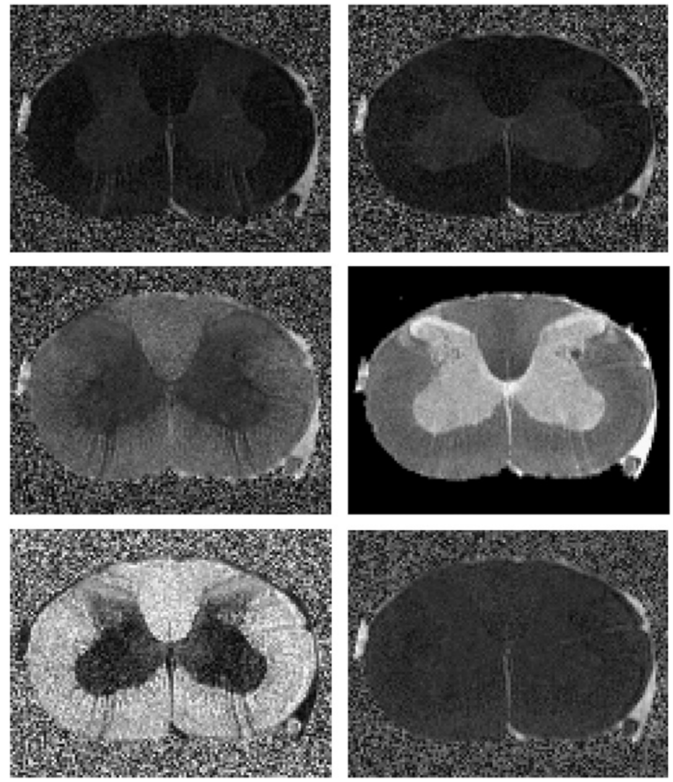

Fig. 3. From left to right, top to bottom are D11, D22, D33, S_0, FA, and mean trace of the estimated tensor field by using MRE on the rat cord data set.

equipped with an 8-channel head array coil. The twice-refocused spin-echo EPI sequence (TR = 12 s, TE = 100 ms) consists of 22 diffusion gradients with a b-value of $800 s/mm^2$.

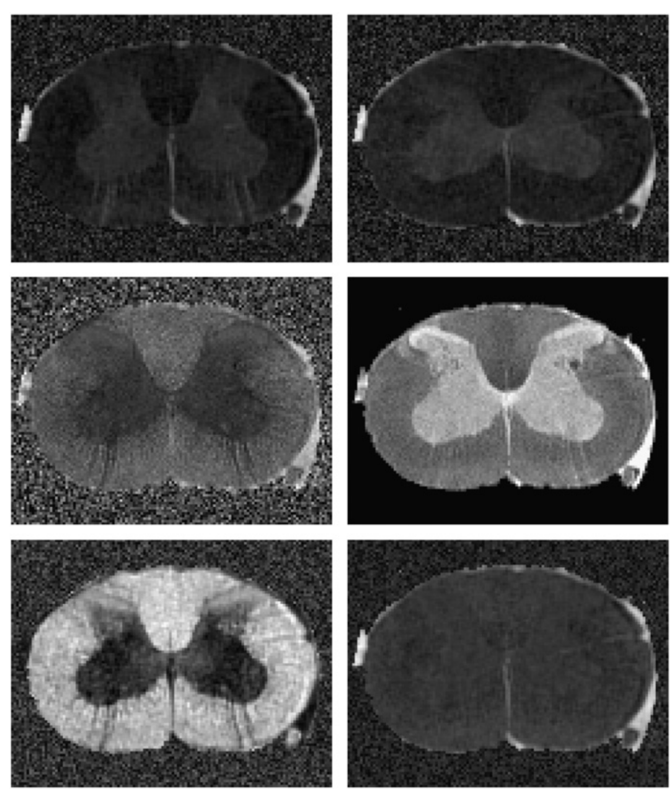

Fig. 4. From left to right, top to bottom are D11, D22, D33, S_0, FA, and mean trace of the estimated tensor field by using LMMSE on the rat cord data set.

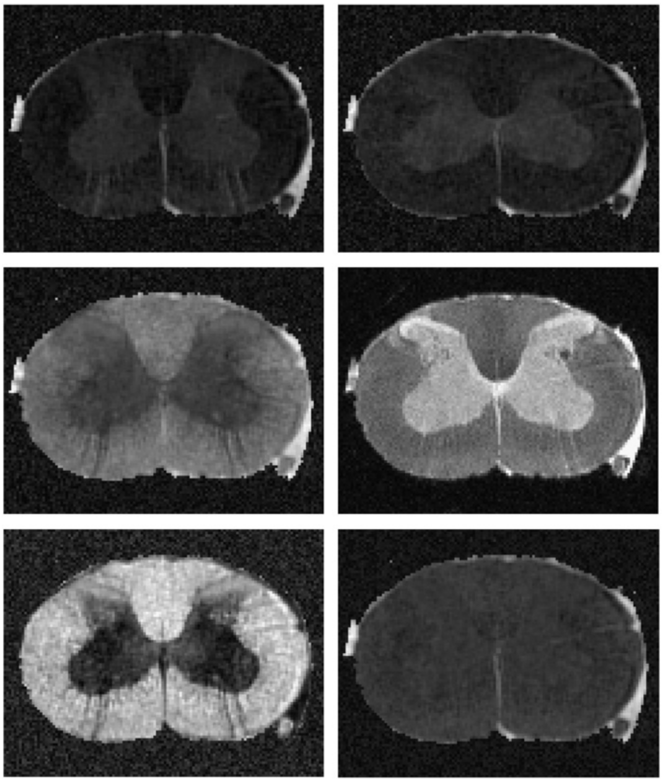

Fig. 5. From left to right, top to bottom are D11, D22, D33, S_0, FA, and mean trace of the estimated tensor field by using our proposed method on the rat cord data set.

For the parameters of our model, we chose $\alpha = 0.15$ and $\beta = 0.45$. The search window size is 64 and the neighborhood size is 27. We compared with several other methods on the DTI estimation, however, to save space, we only show the results of MRE, LMMSE and our proposed method. We present D11, D22, D33, S_0, FA, and mean trace for each estimated result. The DTI estimation results of MRE, LMMSE and our proposed method are shown in Figs. 6, 7 and 8 respectively. The comparisons indicate that the proposed DTI estimation method generates better results.

Conclusions

We proposed a robust variational non-local means based unified approach for simultaneous denoising and DTI estimation. The proposed method is a combination of a variational framework, non-local means and an intrinsically robust divergence measure to regularize the DTI estimation. In the variational principle, we used non-linear diffusion tensor fitting term, along with a combination of non-local means and the tKL based smoothness measure for denoising. To speed up the NLM method, we performed prefiltering on the voxels in the search window to reduce the number of computations and made use of parallel computing to distribute the computational load. This variational non-local approach was validated with both synthetic and real datasets and was shown to be more accurate than competing methods in the literature. The results show that our method depicts better noise removal while preserving the structure information even at high levels of noise.

For future work, we plan to develop a GPU-based implementation to further reduce the computation time. After getting a more comprehensive tensor estimation technique, we will utilize it as a preprocessing step in applications to fiber tracking and DTI segmentation.

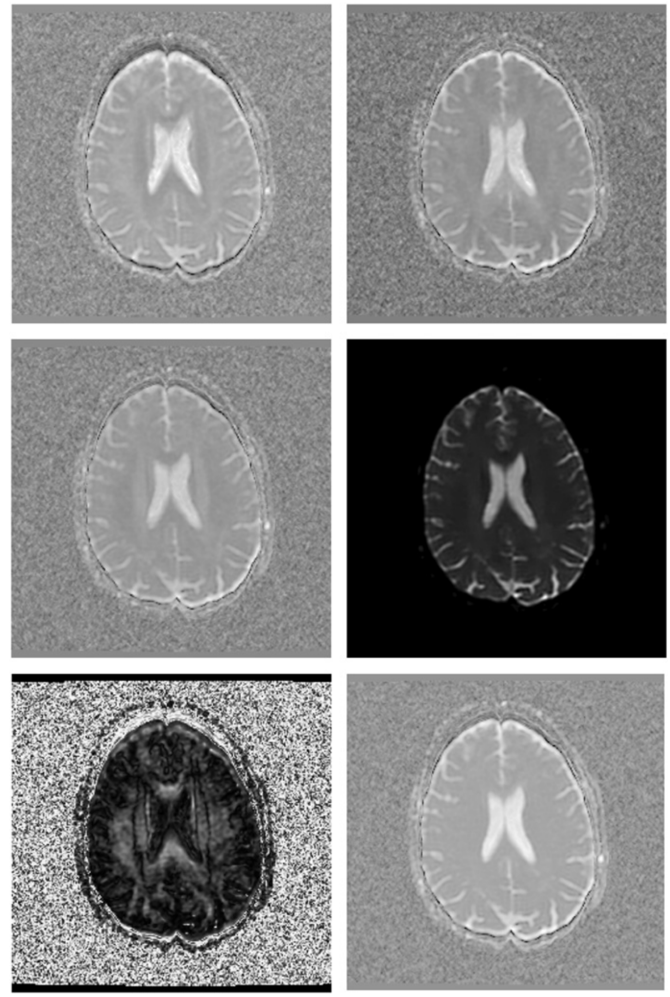

Fig. 6. From left to right, top to bottom are D11, D22, D33, S_0, FA, and mean trace of the estimated tensor field by using MRE on the human brain dataset.

Acknowledgments

This work was in part supported by the NIH grant NS066340 to Vemuri, the University of Florida Allumni Fellowship and the INRIA Internships program to Liu, the Association France Parkinson and the ANR NucleiPark project (French National Research Agency ANR, Neurodegenerative and Psychiatric Diseases program) to Deriche.

We thank Dr. Alfred Anwander of the Max Planck Institute for providing the human brain datasets and Dr. John Forder of the Department of Radiology, University of Florida, McKnight Brain Institute for providing the rat spinal cord datasets.

Appendix A. Automatically ensuring the positivity of *diag*(L)

Since

$$\mathbf{L} = \begin{pmatrix} \mathbf{L}_{11} & 0 & 0 \\ \mathbf{L}_{21} & \mathbf{L}_{22} & 0 \\ \mathbf{L}_{31} & \mathbf{L}_{32} & \mathbf{L}_{33} \end{pmatrix},$$

and

$$\mathbf{D} = \mathbf{L}\mathbf{L}^T = \begin{pmatrix} \mathbf{L}_{11}^2 & \mathbf{L}_{11}\mathbf{L}_{21} & \mathbf{L}_{11}\mathbf{L}_{31} \\ \mathbf{L}_{11}\mathbf{L}_{21} & \mathbf{L}_{21}^2 + \mathbf{L}_{22}^2 & \mathbf{L}_{21}\mathbf{L}_{31} + \mathbf{L}_{21}\mathbf{L}_{32} \\ \mathbf{L}_{11}\mathbf{L}_{31} & \mathbf{L}_{21}\mathbf{L}_{31} + \mathbf{L}_{21}\mathbf{L}_{32} & \mathbf{L}_{31}^2 + \mathbf{L}_{32}^2 + \mathbf{L}_{33}^2 \end{pmatrix}.$$

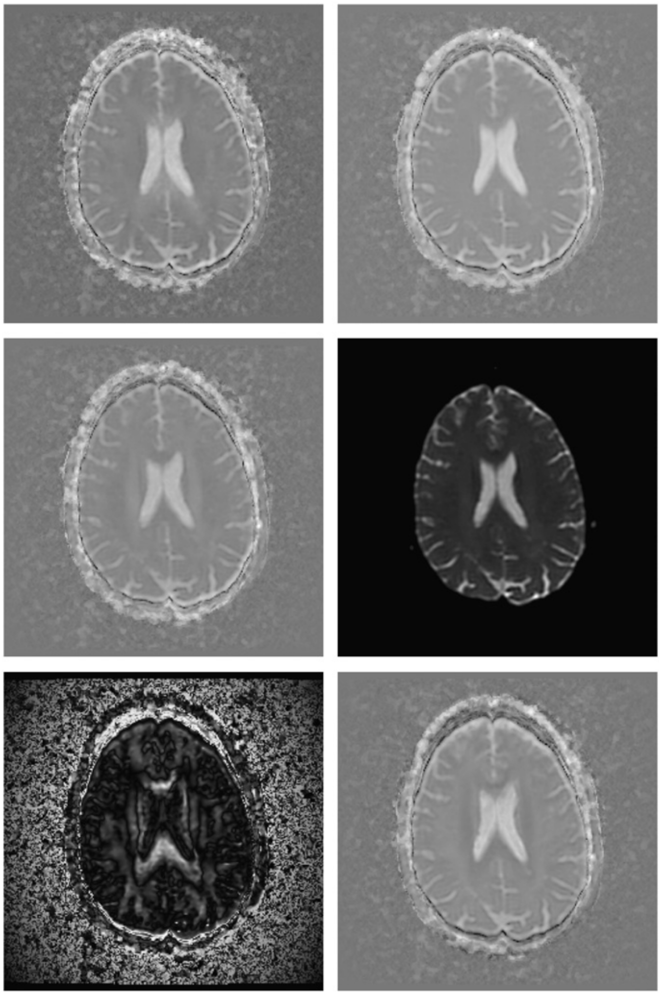

Fig. 7. From left to right, top to bottom are D11, D22, D13, S_0, FA, and mean trace of the estimated tensor field by using LMMSE on the human brain dataset.

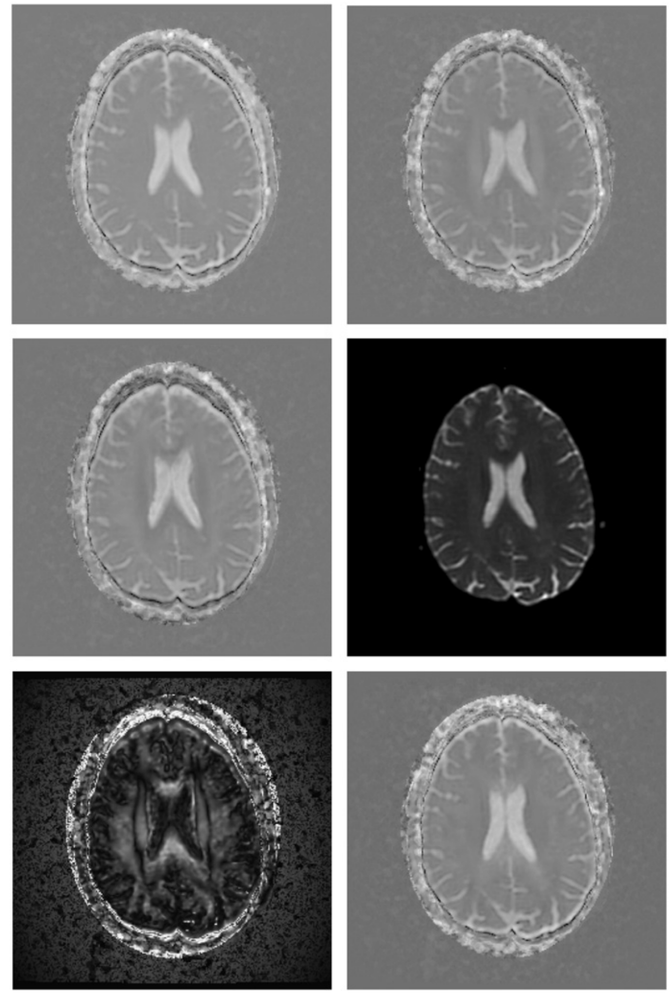

Fig. 8. From left to right, top to bottom are D11, D22, D33, S_0, FA, and mean trace of the estimated tensor field by using our proposed method on the human brain dataset.

Let $\mathbf{L}_{ii} = \exp(a_i)$, $i = 1, 2, 3$, then by solving a_i, we can ensure the $\mathbf{L}_{ii}$ is positive. Therefore, the positiveness of the diagonal values of $\mathbf{L}$ is transferred to solve a_i.

Now $\mathbf{L}$ is converted to $\hat{\mathbf{L}}$:

$$\hat{\mathbf{L}} = \begin{pmatrix} \exp(a_1) & 0 & 0 \\ \mathbf{L}_{21} & \exp(a_2) & 0 \\ \mathbf{L}_{31} & \mathbf{L}_{32} & \exp(a_3) \end{pmatrix}.$$

$$\begin{aligned} \frac{\partial \mathbf{E}}{\partial \mathbf{L}} &= 4(1-\alpha-\beta)\sum_{i=1}^{n} bS_0 v_i \mathbf{L}^T \mathbf{g}_i \mathbf{g}_i^T \\ &\quad -2\beta \sum_{\mathbf{y}\in\mathbb{V}(\mathbf{x})} w_2(\mathbf{x},\mathbf{y}) \frac{\left(\mathbf{L}^{-1} - \mathbf{L}^T \mathbf{L}^{-T}(y)\mathbf{L}^{-1}(y)\right)}{\sqrt{c_1 + \frac{\left(\sum_{i=1}^{3} \log \mathbf{L}_{ii}(\mathbf{y})\right)^2}{4} - c_2 \sum_{i=1}^{3} \log \mathbf{L}_{ii}(\mathbf{y})}}, \\ \frac{\partial \mathbf{E}}{\partial \hat{\mathbf{L}}} &= \frac{\partial \mathbf{E}}{\partial \mathbf{L}} \cdot \mathbf{J}, \end{aligned} \tag{A.1}$$

where "·" is element-wise product, and

$$\mathbf{J} = \begin{pmatrix} \exp(a_1) & 0 & 0 \\ 1 & \exp(a_2) & 0 \\ 1 & 1 & \exp(a_3) \end{pmatrix}.$$

Therefore, the partial derivative is in closed form. This can be solved by using the L-BFGS method.

References

Aja-Fernandez, S., Alberola-Lopez, C., Westin, C.F., 2008. Noise and signal estimation in magnitude MRI and Rician distributed images: a LMMSE approach. IEEE Trans. Image Process. 17 (8), 1383–1398.

Aja-Fernandez, S., Tristan-Vega, A., Alberola-Lopez, C., 2009. Noise estimation in single- and multiple-coil magnetic resonance data based on statistical models. Magn. Reson. Imaging 27, 1397–1409.

Assemlal, H., Tschumperle, D., Brun, L., Siddiqi, K., 2011. Recent advances in diffusion MRI modeling: angular and radial reconstruction. Med. Image Anal. 15 (4), 369–396.

Awate, S., Whitaker, R., 2005. Nonparametric neighborhood statistics for MRI denoising. Inf. Process. Med. Imaging 3565, 677–688.

Barmpoutis, A., Hwang, M.S., Howland, D., Forder, J.R., Vemuri, B.C., 2009a. Regularized positive-definite fourth-order tensor field estimation from DW-MRI. Neuroimage 45 (1), 153–162.

Barmpoutis, A., Jian, B., Vemuri, B.C., 2009b. Adaptive kernels for multi-fiber reconstruction. Inf. Process. Med. Imaging 338–349.

Barmpoutis, A., Vemuri, B.C., 2009. Groupwise Registration and Atlas Construction of 4th-order Tensor Fields Using the Riemannian Metric: MICCAI, 1, pp. 640–647.

Basser, P., Mattiello, J., LeBihan, D., 1994. Estimation of the effective self-diffusion tensor from the NMR spin echo. J. Magn. Reson. 103 (3), 247–254.

Basu, S., Fletcher, T., Whitaker, R., 2006. Rician noise removal in diffusion tensor MRI. MICCAI, pp. 117–125.

Batchelor, P.G., Moakher, M., Atkinson, D., Calamante, F., Connelly, A., 2005. A rigorous framework for diffusion tensor calculus. Magn. Reson. Med. 53 (1), 221–225.

Landman, Bennett A., B., P.-L., P., J.L., 2007. Diffusion tensor estimation by maximizing Rician likelihood. IEEE ICCV, pp. 1–8.

Burgela, U., Amuntsb, K., Hoemkec, L., Mohlbergc, H., Gilsbacha, J.M., Zilles, K., 2006. White matter fiber tracts of the human brain: Three-dimensional mapping at microscopic resolution, topography and intersubject variability. Neuroimage 29 (4), 1092–1105.

Chang, L.-C., Jones, D.K., Pierpaoli, C., 2005. RESTORE: robust estimation of tensors by outlier rejection. Magn. Reson. Med. 53, 1088–1095.

Chefd'hotel, C., Tschumperle, D., Deriche, R., Faugeras, O., 2004. Regularizing flows for constrained matrix valued images. J. Math. Imaging Vis. 20 (1–2), 147–162.

Coupe, P., Yger, P., Barillot, C., 2006. Fast non local means denoising for 3D MR images. MICCAI, pp. 33–40.
Coupe, P., Yger, P., Prima, S., Hellier, P., Kervrann, C., Barillot, C., 2008. An optimized blockwise non local means denoising filter for 3D magnetic resonance images. IEEE Trans. Med. Imaging 27 (4), 425–441.
Descoteaux, M., Wiest-Daessl, N., Prima, S., Barillot, C., Deriche, R., 2008. Impact of Rician adapted non-local means filtering on HARDI. MICCAI, pp. 122–130.
DeVore, M.D., Lanterman, A.D., OSullivan, J.A., 2000. ATR performance of a Rician model for SAR images. Proc. SPIE, pp. 34–37.
Durrleman, S., Fillard, P., Pennec, X., Trouve, A., Ayache, N., 2011. Registration, atlas estimation and variability analysis of white matter fiber bundles modeled as currents. Neuroimage.
Faugeras, O., Adde, G., Charpiat, G., Chefd'Hotel, C., Clerc, M., Deneux, T., Deriche, R., Hermosillo, G., Keriven, R., Kornprobst, P., Kybic, J., Lenglet, C., Lopez-Perez, L., Papadopoulo, T., Pons, J., Segonne, F., Thirion, B., Tschumperlé, D., Viéville, T., Wotawa, N., 2004. Variational, geometric and statistical methods for modeling brain anatomy and function. Neuroimage 23 (1), S46–S55.
Fillard, P., Arsigny, V., Pennec, X., Thompson, P.M., Ayache, N., 2005. Extrapolation of sparse tensor fields: application to the modeling of brain variability. Inf. Process. Med. Imaging 19, 27–38.
Fillard, P., Descoteaux, M., Goh, A., Gouttard, S., Jeurissen, B., Malcolm, J., Ramirez-Manzanares, A., Reisert, M., Sakaie, K., Tensaouti, F., Yo, T., Mangin, J.F., Poupon, C., 2011. Quantitative evaluation of 10 tractography algorithms on a realistic diffusion MR phantom. Neuroimage 56 (1), 220–234.
Fillard, P., Pennec, X., Arsigny, V., Ayache, N., 2007. Clinical DT-MRI estimation, smoothing, and fiber tracking with log-Euclidean metrics. IEEE Trans. Med. Imaging 26 (11), 1472–1482.
Gilboa, G., Sochen, N., Zeevi, Y.Y., 2004. Image enhancement and denoising by complex diffusion processes. IEEE Trans. Pattern Anal. Mach. Intell. 26 (8), 1020–1036.
Goh, A., Vidal, R., 2008. Segmenting fiber bundles in diffusion tensor images. ECCV 24 (10), 238–250.
Golub, G.H., Loan, C.F.V., 1996. Matrix Computations. JHU Press.
Gur, Y., Sochen, N., 2007. Fast invariant Riemannian DT-MRI regularization. ICCV, pp. 1–7.
Hamarneh, G., Hradsky, J., 2007. Bilateral filtering of diffusion tensor magnetic resonance images. IEEE Trans. Image Process. 16, 2463–2475.
Hasan, K.M., Halphen, C., Sankar, A., Eluvathingal, T.J., Kramer, L., Stuebing, K.K., Ewing-Cobbs, L., Fletcher, J.M., 2007. Diffusion tensor imaging based tissue segmentation: validation and application to the developing child and adolescent brain. Neuroimage 34 (4), 1497–1505.
Jia, H., Yap, P., Wu, G., Wang, Q., Shen, D., 2011. Intermediate templates guided groupwise registration of diffusion tensor images. Neuroimage 54, 928–939.
Jones, D.K., 2010. Diffusion MRI Theory, Methods, and Applications. Oxford University Press.
Koay, C.G., Basser, P.J., 2006. Analytically exact correction scheme for signal extraction from noisy magnitude MR signals. J. Magn. Reson. 179 (2), 317–322.
Lenglet, C., Prados, E., Pons, J., Deriche, R., Faugeras, O., 2009. Brain connectivity mapping using Riemannian geometry, control theory and PDEs. SIAM J. Imaging Sci. 2 (2), 285–322.
Lenglet, C., Rousson, M., Deriche, R., 2006. DTI segmentation by statistical surface evolution. IEEE Trans. Med. Imaging 25 (6), 685–700.
Liu, M., Vemuri, B.C., Amari, S.-I., Nielsen, F., 2010. Total Bregman divergence and its applications to shape retrieval. IEEE CVPR, pp. 3463–3468.
Liu, T., Li, H., Wong, K., Tarokh, A., Guo, L., Wong, S.T., 2007. Brain tissue segmentation based on DTI data. Neuroimage 38 (1), 114–123.
Makuuchi, M., Bahlmann, J., Anwander, A., Friederici, A.D., 2009. Segregating the core computational faculty of human language from working memory. Proc. Natl. Acad. Sci. U.S.A. 106 (20), 8362–8367.
Mangin, J.F., Poupon, C., Clark, C., Le Bihan, D., Bloch, I., 2002. Distortion correction and robust tensor estimation for MR diffusion imaging. Med. Image Anal. 6 (3), 191–198.
Manjon, J.V., Carbonell-Caballero, J., Lull, J.J., García-Marti, G., Marti-Bonmati, L., Robles, M., 2008. MRI denoising using non-local means. Med. Image Anal. 12, 514–523.
Martin-Fernandez, M., Alberola-Lopez, C., Ruiz-Alzola, J., Westin, C.F., 2007. Sequential anisotropic wiener filtering applied to 3D MRI data. Magn. Reson. Imaging 25, 278–292.
Marzetta, T., 1995. EM Algorithm for Estimating the Parameters of Multivariate Complex Rician Density for Polarimetric SAR: Procs. of ICASSP, 5, pp. 3651–3654.
McGibney, G., Smith, M., 1993. Unbiased signal to noise ratio measure for magentic resonance images. Med. Phys. 20 (4), 1077–1078.
McGraw, T., Vemuri, B.C., Chen, Y., Rao, M., Mareci, T., 2004. DT-MRI denoising and neuronal fiber tracking. Med. Image Anal. 8, 95–111.
Mishra, A., Lu, Y., Meng, J., Anderson, A.W., Ding, Z., 2006. Unified framework for anisotropic interpolation and smoothing of diffusion tensor images. Neuroimage 31 (4), 1525–1535.
Moraga, C.C., Lenglet, C., Deriche, R., Ruiz-Alzola, J., 2007. A Riemannian approach to anisotropic filtering of tensor fields. Signal Process. 87 (2), 217–352.
Mori, S., Oishi, K., Jiang, H., Jiang, L., Li, X., Akhter, K., Hua, K., Faria, A., Mahmood, A., Woods, R., Toga, A., Pike, G., Neto, P., Evans, A., Zhang, J., Huang, H., Miller, M., van Zijl, P., Mazziotta, J., 2008. Stereotaxic white matter atlas based on diffusion tensor imaging in an ICBM template. Neuroimage 40 (2), 570–582.
Mori, S., van Zijl, P.C., 2002. Fiber tracking: principles and strategies — a technical review. NMR Biomed. 15 (7), 464–480.
Motwani, K., Adluru, N., Hinrichs, C., Alexander, A.L., Singh, V., 2010. Epitome driven 3-D diffusion tensor image segmentation: on extracting specific structures. NIPS, pp. 1696–1704.
Niethammer, M., Estepar, R.S.J., Bouix, S., Shenton, M., Westin, C.-F., 2006. On diffusion tensor estimation. Conf. Proc. IEEE Eng. Med. Biol. Soc. 1, 2622–2625.
Nocedal, J., Wright, S.J., 2000. Numerical Optimization. Springer.
Nowak, R., 1999. Wavelet-based Rician noise removal for magnetic resonance imaging. IEEE Trans. Image Process. 8 (10), 1408–1419.
Pennec, X., Fillard, P., Ayache, N., 2006. A Riemannian framework for tensor computing. Int. J. Comput. Vis. 66 (1), 41–66.
Piurica, A., Philips, W., Lemahieu, I., Acheroy, M., 2003. A versatile wavelet domain noise filtration technique for medical imaging. IEEE Trans. Med. Imaging 22 (3), 323–331.
Poupon, C., Rieul, B., Kezele, I., Perrin, M., Poupon, F., Mangin, J., 2008a. New diffusion phantoms dedicated to the study and validation of high-angular-resolution diffusion imaging (HARDI) models. Magn. Reson. Med. 60, 1276–1283.
Poupon, C., Roche, A., Dubois, J., Mangin, J.-F., Poupon, F., 2008b. Real-time MR diffusion tensor and Q-ball imaging using Kalman filtering. Med. Image Anal. 12, 527–534.
Salvador, R., Pena, A., Menon, D.K., Carpenter, T.A., Pickard, J.D., Bullmore, E.T., 2005. Formal characterization and extension of the linearized diffusion tensor model. Hum. Brain Mapp. 24 (2), 144–155.
Savadjiev, P., Campbell, J.S.W., Descoteaux, M., Deriche, R., Pike, G.B., Siddiqi, K., 2008. Labeling of ambiguous subvoxel fibre bundle configurations in high angular resolution diffusion MRI. Neuroimage 41 (1), 58–68.
Sijbers, J., den Dekker, A., 2004. Maximum likelihood estimation of signal amplitude and noise variance from MR data. Magn. Reson. Imaging 51 (3), 586–594.
Spira, A., Kimmel, R., Sochen, N., 2007. A short-time Beltrami kernel for smoothing images and manifolds. IEEE Trans. Image Process. 16 (6), 1628–1636.
Stejskal, E.O., Tanner, J.E., 1965. Spin diffusion measurements: spin echoes in the presence of a time-dependent field gradient. J. Chem. Phys. 42, 288–292.
Tang, S., Fan, Y., Zhu, H., Yap, P., Gao, W., Lin, W., Shen, D., 2009. Regularization of diffusion tensor field using coupled robust anisotropic diffusion. MMBIA, pp. 52–57.
Tristan-Vega, A., Aja-Fernandez, S., 2010. DWI filtering using joint information for DTI and HARDI. Med. Image Anal. 14 (2), 205–218.
Tschumperle, D., Deriche, R., 2003. Variational Frameworks for DT-MRI Estimation, Regularization and Visualization: IEEE ICCV, 1, pp. 116–121.
Tschumperle, D., Deriche, R., 2005. Vector-valued image regularization with PDEs: a common framework for different applications. IEEE Trans. Pattern Anal. Mach. Intell. 27 (4), 506–517.
Vemuri, B.C., Chen, Y., Rao, M., McGraw, T., Wang, Z., Mareci, T., 2001. Fiber tract mapping from diffusion tensor MRI. Proceedings. IEEE Workshop on Variational and Level Set Methods in Computer Vision (VLSM), pp. 81–88.
Vemuri, B.C., Liu, M., Amari, S.-I., Nielsen, F., 2011. Total Bregman divergence and its applications to DTI analysis. IEEE Trans. Med. Imaging 30 (2), 475–483.
Wang, Q., Yap, P., Wu, G., Shen, D., 2012. Application of neuroanatomical features to tractography clustering. Hum. Brain Mapp.
Wang, Y., Gupta, A., Liu, Z., Zhang, H., Escolar, M.L., Gilmore, J.H., Gouttard, S., Fillard, P., Maltbie, E., Gerig, G., Styner, M., 2011. DTI registration in atlas based fiber analysis of infantile Krabbe disease. Neuroimage 55 (4), 1577–1586.
Wang, Y., Zhang, J., Gutman, B., Chan, T.F., Becker, J.T., Aizenstein, H.J., Lopez, O.L., Tamburo, R.J., Toga, A.W., Thompson, P.M., 2010. Multivariate tensor-based morphometry on surfaces: application to mapping ventricular abnormalities in HIV/AIDS. Neuroimage 49 (3), 2141–2157.
Wang, Z., Vemuri, B.C., 2005. DTI segmentation using an information theoretic tensor dissimilarity measure. IEEE Trans. Med. Imaging 24 (10), 1267–1277.
Wang, Z., Vemuri, B.C., Chen, Y., Mareci, T., 2003. A constrained variational principle for direct estimation and smoothing of the diffusion tensor field from DWI. Inf. Process. Med. Imaging 2732/2003, 660–671.
Wang, Z., Vemuri, B.C., Chen, Y., Mareci, T.H., 2004. A constrained variational principle for direct estimation and smoothing of the diffusion tensor field from complex DWI. IEEE Trans. Med. Imaging 23, 930–939.
Westin, C.F., Maier, S., Mamata, H., Nabavi, A., Jolesz, F., Kikinis, R., 2002. Processing and visualization for diffusion tensor MRI. Med. Image Anal. 6, 93–108.
Wiest-Daessle, N., Prima, S., Coupé, P., Morrissey, S.P., Barillot, C., 2008. Rician noise removal by non-local means filtering for low signal-to-noise ratio MRI: applications to DT-MRI. MICCAI, pp. 171–179.
Xie, Y., Vemuri, B.C., Ho, J., 2010. Statistical Analysis of Tensor Fields: MICCAI, 1, pp. 682–689.
Yang, J., Shen, D., Davatzikos, C., Verma, R., 2008. Diffusion tensor image registration using tensor geometry and orientation features. MICCAI, pp. 905–913.
Yeo, B., Vercauteren, T., Fillard, P., Peyrat, J.-M., Pennec, X., Golland, P., Ayache, N., Clatz, O., 2009. DT-REFinD: diffusion tensor registration with exact finite-strain differential. IEEE Trans. Med. Imaging 28 (12), 1914–1928.
Zhang, Y., Brady, M., Smith, S., 2001. Segmentation of brain MR images through a hidden Markov random field model and the expectation–maximization algorithm. IEEE Trans. Med. Imaging 2 (1), 45–57.
Zhu, H., Kong, L., Li, R., Styner, M., Gerig, G., Lin, W., Gilmore, J.H., 2011. FADTTS: functional analysis of diffusion tensor tract statistics. Neuroimage 56 (3), 1412–1425.